HEAT AND MASS TRANSFER MECHANISMS AT WAVY GAS-LIQUID INTERFACES

Valerio De Angelis
Department of Chemical Engineering
University of California Santa Barbara
Santa Barbara (CA), 93106

Sanjoy Banerjee
Department of Chemical Engineering
University of California Santa Barbara
Santa Barbara (CA), 93106

ABSTRACT

Mass transfer across a wavy interface has been investigated by mean of direct numerical simulation. Gas and liquid streams, with physical properties typical of air and water, flow counter-currently. Two cases are presented. In the first, the interface is kept flat in the limit of low Froude and Weber number. The results of this simulation elucidate the effect of turbulence on mass transfer without the complication introduced by waves. In the second case, the interface is free to deform and waves in the capillary and capillary-gravity range can form. The simulation corresponds to a ten-meter wind velocity of $\sim$ 7 m/s. The simulations are for values of the Schmidt number up to 100.

The values of mass transfer velocity obtained from the simulation are in good agreement with laboratory experiments. Waves do not significantly affect mass transfer velocity non dimensionalized by the interfacial frictional velocity. On the liquid side, high mass transfer regions over the interface correlate well with sweeps on the liquid side for all values of the Schmidt number. On the gas side, mass transfer velocity correlates well with sweeps for moderate values of Schmidt number. For high values of Schmidt, however, all turbulence events with significant interface-normal velocity become relevant.

Based on these mechanisms, parametrizations for the mass transfer velocity are proposed, based only on the characteristics of the turbulence structures and without adjustable parameters. They compare well with experiments and indicate that it is the turbulence, rather than the waves characteristics, that controls mass transfer.

PROBLEM DESCRIPTION

In order to better understand the mechanisms of mass transfer at gas-liquid interfaces, it is important to investigate the microphysics of transport processes dominated by fine-scale turbulence *e.g.* in gas exchange. Such phenomena are controlled, for wind speed below those at which wave breaking occurs, by layers $\sim$O(0.01 mm) on the liquid side and $\sim$O(1 mm) on the gas side. On these scales, ripples and capillary waves with wavelengths $\sim$O(1 cm) can perhaps impact scalar transfer, but larger wavelengths have little effect.

Since scalar transfer at continuous interfaces occurs over length scales that lead to relatively low Reynolds numbers when these are based on thicknesses of the layers containing the main resistances, Direct Numerical Simulation (DNS) may well clarify the important transport mechanisms for such problems.

In Lombardi *et al.* (1996) interaction of air and water across a flat interface was investigated to study the coupling between the fluids without the complexity of interface deformation. In this manuscript we extend those results and discuss the properties of mass transfer for relatively high Schmidt number ($\sim$ 100). We also account for the effect of capillary waves. The region of wave spectrum that is simulated has wavelengths comparable to, or smaller than, the typical lengths scales of the turbulence structures. These waves can interact with the underlying turbulence and affect mass transfer across the interface.

For reasons of space, we do not report details of the numerical algorithm. These can be found in De Angelis (1998). In Figure 1 the domain geometry is shown. Gas and liquid flow countercurrently, and they interact at the interface that deforms under the effect of the

flow with the deformations moderated by gravitational forces and surface tension.

At each step the velocity, pressure and a scalar field (concentration or temperature) are calculated without any turbulence model. The simulations are for a Re_τ of 171, when based on the heights of each domain and the shear velocity at the interface $u_\tau = \sqrt{\tau_I/\rho}$. The Schmidt number $Sc = \nu/D$ is varied in steps between 1 and 100.

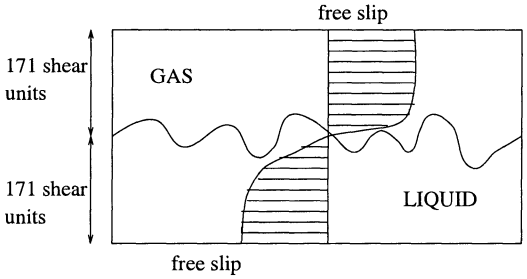

Figure 1: Geometry of the Simulation

FLAT INTERFACE

Consider, first, conditions set to keep the liquid Froude number and the gas velocity low enough to be well away from instabilities. A non-wavy surface can be obtained even when quite high shear rates are imposed, as shown experimentally by Rashidi and Banerjee (1990). This situation has been studied by Lombardi *et al.* (1996) with regard to the momentum coupling across the interface. We now discuss the effect of turbulence structure on mass transfer.

Runs at different density ratios ($R^2 = \frac{\rho_L}{\rho_g}$) between the fluids are discussed in Lombardi *et al.* (1996). In here we summarize for clarity some important results for case R29, *i.e.* R=29.9, typical of air-water flows.

The interfacial plane itself shows regions of high shear stress and low shear stress, with low shear stress regions corresponding to the low speed regions and the high shear stress to the high speed regions. The low shear stress regions are streaky in nature with high shear stress islands. At the edges of the high shear stress regions, vortices are seen to spin up on both sides of the interface. These are initially in the plane normal to the interface but subsequently are stretched in the quasi-streamwise direction by the mean flow. These quasi-streamwise vortices are known to play a major role in the ejection-sweep processes observed in wall turbulence, and they do the same at the gas-liquid interface.

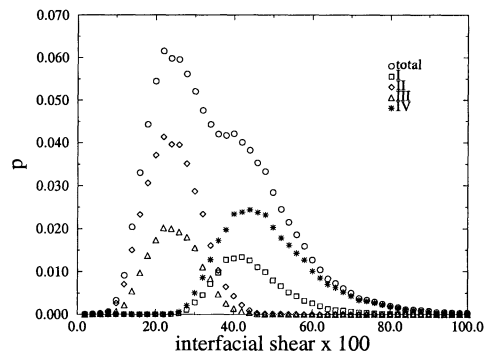

a): Gas side

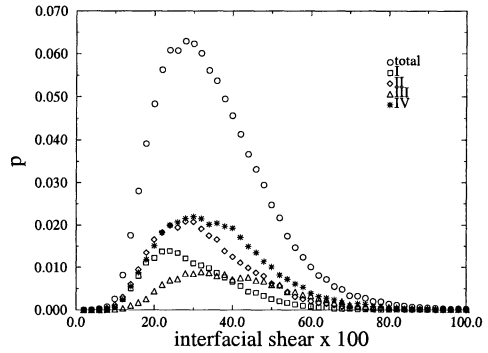

b): Liquid side

Figure 2: Quadrant analysis of $u'w'$ with stress.

The formation of the high shear stress regions can be clarified by considering a quadrant analysis of the velocity field over the interface in which velocity fluctuations in each quadrant of the Reynolds stresses are correlated with shear stress at the interface. In the first quadrant both the streamwise and interface normal velocity fluctuations are positive. In the second, the streamwise component is negative but the interface normal component is positive. This corresponds to an ejection of low speed fluid. In the third quadrant both the streamwise and the interface-normal velocity fluctuations are negative, and in the fourth the streamwise component is positive whereas the interface-normal component is negative. The fourth quadrant then corresponds to a sweep in which high-speed fluid is brought towards the interface. Consider now the correlation of each quadrant of such velocity fluctuations with the interfacial shear stress shown in Figure 2.a on the gas side. It is clear that sweeps, i.e., in the fourth quadrant, lead to the high shear stress regions whereas ejections lead to the low shear stress regions. This is what is observed in wall turbulence at a solid boundary and therefore the gas sees the liquid surface much like a solid boundary. However, if we look at Figure 2.b, it is immediately clear that no such correlation exists on the liquid side. In fact, all the quadrants have similar behavior with regard to the shear stress regions that occur below the high speed sweeps on the gas side, *i.e.* , the motions

that bring high speed fluid from the outer regions to the interfaces on the gas side leads to high shear stress at the interface. Conversely, ejections on the gas side which take low speed fluid away from the interface into the outer flow, strongly correlate with low shear stress regions. The liquid does not behave in this way and does not dominate the pattern of shear stress on the interface.

The difference between the gas and the liquid phases in the near interface region is further clarified by observing the velocity fluctuations on each side of the interface (Lombardi *et al.* , 1996). The gas behaves much like flow over a solid wall. The fluctuations are almost identical to that at a solid boundary, in all directions – streamwise, spanwise, and wall-normal. On the other hand, the liquid has the largest fluctuations in the streamwise and spanwise directions right at the interface itself. It sees the interface virtually as a free slip boundary, except for the mean shear.

The gas flows over what is essentially a no-slip boundary, the velocity fluctuations at the interface being small compared to the shear velocity. From the continuity equation, $\frac{du_i}{dx_i} = 0$, and assuming $u_1 = u_2 = 0$ at the boundary we obtain that $\frac{du_3}{dx_3} = 0$. On the liquid side, the velocity fluctuations at the interface are not negligible and $\sum_{i=1,2} \frac{du_i}{dx_i} \neq 0$.

It follows that on the gas side $u_{3g} \sim A_2 x_3^2$, whereas on the liquid $u_{3l} \sim A_1 x_3$. The turbulence structure on the liquid side thus penetrates further toward the interface. Using the same scaling arguments we obtain that the Reynolds stresses have to vary, close to the interface, as $\sim B_3 x_3^3$ and $\sim B_1 x_3$ on the gas and liquid sides respectively.

The differences observed in the analysis of the velocity field on the two sides are of some importance for the scalar transfer mechanism on the two sides. We define two non-dimensional mass transfer velocity, β^+ as:

$$\beta^+ = \frac{1}{\sqrt{2} Re_\tau Sc (c_o - c_b)} \frac{du}{dx_3} \quad ; \quad c_b = \frac{\int_0^{2h} \overline{u_1 c} dx_3}{\int_0^{2h} \overline{u_1} dx_3} \quad (1)$$

where $\frac{du}{dx_3}$ is the nondimensional gradient at the interface and c_b and c_o are the bulk and interface concentrations and Re_τ is based on the shear velocity at the interface, $u_\tau = \sqrt{\tau_I / \rho}$.

The values of β^+ on the gas and liquid sides are shown in Figure 3. The value of β^+ scales as $Sc^{-2/3}$ on the gas side and $Sc^{-1/2}$ on the liquid side for the high Sc number cases. This implies that the concentration boundary layer thickness, δ_c, scales as $Sc^{1/3}$ and $Sc^{1/2}$ on the gas and liquid side respectively.

At a continuous interface, in the absence of bubbles or wave breaking, mass transfer takes place by conduction only, therefore it is enhanced when bulk fluid is conveyed to the interface region, *e.g.* by sweeps, or when ejections of fluid remove saturated fluid.

We then extend the quadrant analysis of Figure 2 and look at the correlation of the Reynolds stress – and therefore of the turbulence structure, in the various quadrants with the instantaneous value of mass transfer velocity β^+ at the interface. The Reynolds stresses, for all the Sc numbers, are always sampled within the first 12 shear units, *e.g.* the regions of high turbulent energy production, regardless of the thickness of the concentration boundary layer.

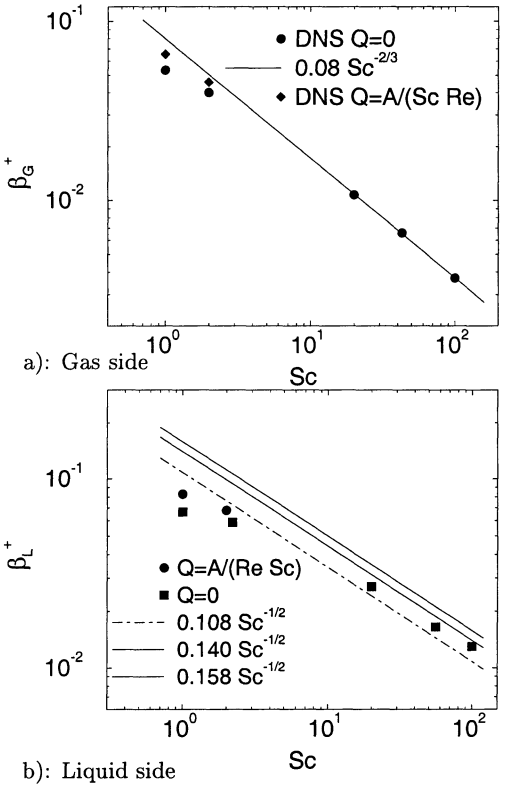

Figure 3: Mass transfer velocity at the interface

Results are reported in De Angelis (1998) for Sc=1 and Sc=100 on the gas and liquid sides, and summarized here. On the liquid side sweeps correlate with the highest values of β^+ at the interface for both values of the Schmidt number. On the gas side, for low Schmidt number, I and IV quadrant events correlate well with high β^+, but for Sc=100, sweeps and ejections play the dominant role.

The relative importance of the events sorted by quadrants is summarized by in Table I. In the table we report the probability of an event to occur (f_p) and the fraction of the total flux through the interface associated with it (f_h). On the liquid side sweeps carry a larger fraction of mass flux (~ 0.50), than their probability (~ 0.30). The interface can be efficiently renewed by sweeps, the horizontal fluctuations being relatively unimpeded.

On the gas, for the low Schmidt number, sweeps and Quadrant I events are seen to be the most effective for scalar transfer, but when the Schmidt number in-

creases, and the scalar boundary layer becomes thin, sweeps penetrate the concentration layer less, and ejections also become important. The interface-normal velocity fluctuations very close to the interface decrease fast (as $\sim x_3^2$) and control the mass fluxes.

Table I: Reynold stress and total heat fraction corresponding to Quadrant II and IV.

Sc (gas)	1	100	Sc (liq)	1	100
f_p in II	0.36	0.38	f_p in II	0.29	0.32
f_p in IV	0.33	0.32	f_p in IV	0.34	0.37
f_h in II	0.25	0.34	f_h in II	0.15	0.20
f_h in IV	0.46	0.36	f_h in IV	0.52	0.52

We will see how these considerations allow simple parametrizations of β^+ to be developed in a later section.

DEFORMING INTERFACE

When the interface is free to deform two new parameters enter the analysis: the Froude number (Fr) and the Weber number (We), these are defined as $We = \frac{\rho h u_*^2}{\gamma}$ and $Fr = \frac{u_*^2 \rho}{gh(\rho_l - \rho_g)}$

The numerical method cannot handle wave breaking so We and Fr have to be chosen carefully. This limits the shear velocity $\sim$ 0.3 m/s on the gas side which implies for an air-sea problem a 10 m wind velocity of about 7.5 m/s.

In fact, interface deformations depend upon the shear velocity. The shear velocity is related to the undisturbed wind velocity. The cases considered are listed in Table II together with 10 m and 5 m wind velocities obtained by correlations provided by Garrat (1977) and by Komori (1993).

Table II: Matrix of runs performed. Velocities are in m/sec

Case	Fr_τ	We_τ	$u_{\tau g}$	U_5	U_{10}
D0	5.910^{-6}	1.310^{-3}	0.06	2.2	2.2
D1	4.510^{-4}	5.310^{-3}	0.27	5.7	7.6
D2	1.710^{-3}	8.210^{-3}	0.41	7.6	11.0

In case D0 the interface is virtually flat and this serves as reference case. The wave amplitudes in cases D1 are $\sim$O(1 mm) and the wavelength about 2 cm. The computational domain dimensions are roughly 12 cm in the streamwise direction, 6 cm in the spanwise direction and 2 cm in the interface-normal direction. This covers a range of wavenumber, in the flow direction, of 1 cm^{-1} to 15 cm^{-1}. The domain size is sufficient to capture capillary wave effects, and in case D1, waves appear to have reached a equilibrium amplitude and steepness in the capillary wave range. In the D2 case the wind velocity is high. We were able to collect some interesting information before the calculation had to stop.

Case D1 is be used to study the effect of the waves on the average turbulence quantities. Case D2 is be used to study the effect of waves on turbulence structures, because the wave amplitudes are higher than in the other case.

We analyzed the three-dimensional structure of the velocity, shear and pressure field for case D2. The high shear stress regions occur on the wave crests and are again caused by the high-speed fluid on the gas side. In the concave regions the shear is low. Occasionally recirculation on the gas side can be observed.

Pressure is discontinuous on the two sides of the interface, as required by the normal stress boundary condition. On the gas side pressure is lower on the wave crests and high in the wave valleys. On the liquid side, not surprisingly the opposite trend is observed. Even if the patterns of shear stress and pressure are dominated by the form of the waves, streaks are still seen to form on the two sides of the interface. The streak length is not organized on the wave patterns, and the spacing in between streaks is $z^+ \sim 100$, as for wall- and flat-interface turbulence.

Waves do not seem to effect the kinematics of the flow, as observed in the snapshots of the three dimensional velocity fields. This impression is confirmed by the quadrant analysis of Reynolds stresses as function of the shear stress for case D1. These are not shown here. The trend in fact is the same as observed over a flat interface. Sweeps and Quadrant I are more probable on the gas side for high values of the shear stress and ejections and Quadrant III events are more probable for low values of the shear stress. On the liquid side there is no such separation.

The frequency spectrum of the wave amplitude is obtained over a time interval of $T^+ = 350$. It shows a peak for $T^+ = 22$ that corresponds closely to the the frequency peak measured by McCready and Hanratty (1985). Also the peak value is in good agreement. Time spectra of Reynolds stress show instead a peak for $T^+ \sim 50$. For the flat-interface case, the Reynolds stress time spectrum also shows a peak for $T^+ \sim 50$. This values is in good agreement with the sweep and ejection frequency measured by Rashidi and Banerjee (1990). Even when capillary waves form, the main features of the turbulence *i.e.* sweeps and ejections frequency and their behavior with regard to the interfacial stresses, are unchanged.

The maximum wave amplitude in case D1 is $\sim$O(1 mm), that compares well with what Komori *et al.* (1993) report.

Turning now to scalar transfer, we do not observe significant changes in the value of β^+ on the gas and liquid side with respect to the flat interface case. Changes are of O(5-10%) which is within the statistical error. Having said this, we do observe a slight trend. The value of β^+ on the liquid side is seen to increase with wave amplitude. On the gas side the values decrease. Results are shown in Figure 6 as a function of Sc number for

case D1 and compared to the D0 case.

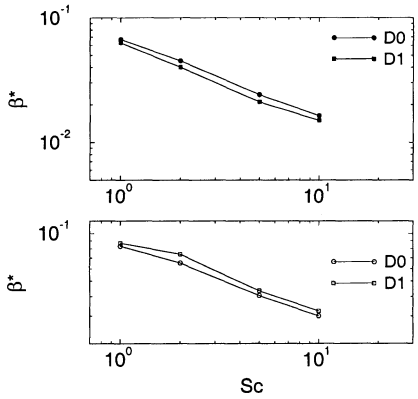

Figure 6: β^+ for gas (top) and liquid (bottom).

The modest increase of β^+ for small wave amplitude on the liquid side has also been observed by Komori *et al.* (1993) in wind-wave tank experiments. Komori *et al.* (1993) observed first a slight increase of β^+ with wave amplitude, and then a drop, for wind speed not covered by our calculations.

As shown in De Angelis (1998), the Reynolds stresses show, on the gas and liquid sides, only modest differences between the D0 (flat) and D1 (wavy) interface cases. Because from our analysis it appears that it is the value and behavior of the Reynolds stresses that affects the values of the mass transfer velocity, the small differences observed in the mass transfer velocity are not surprising.

MASS TRANSFER MODELING

We will now show how simple parametrizations based on surface renewal can capture the mass transfer velocity at an interface. Surface renewal theory hypothesizes that the mass flux across an interface is governed by renewals of the interfacial fluid by motion of the bulk fluid. Scalar transfer proceeds by unsteady diffusion into renewed regions of the surface till the fluid is replenished and the process starts again. A simple expression for the scalar transfer velocity results that involves the renewal frequency. However the issue is to determine the frequency of such renewals. DNS can inform the debate regarding the controlling mechanisms, because essentially every quantity of importance is computed and available for the development of simple models.

In applying surface renewal theory to mass transfer at the interface it is important to remember that the interface travels with the liquid flow with a velocity of $\sim 4u_\tau$ (Lombardi *et al.* , 1996). Therefore after a sweep impacts the interface and generates a region of high mass flux, then that region will move with the interface. The time decay of the mass transfer coefficient has, therefore, to be observed in a Lagrangian frame, *i.e.* moving with the interface. We observed, in fact, that high mass flux regions travel on the interface a distance as long as $\sim$ 300 shear based units, before the high driving force established by a sweep is extinguished.

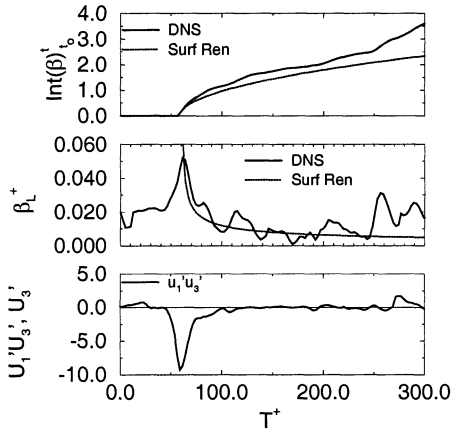

Figure 7: Surface Renewal theory.

In Figure 7 we show a comparison between the DNS results and the prediction of surface renewal theory on the liquid side for Sc=56. The results for the surface renewal theory are based on the assumption that the sweeps are the renewal events. When a sweep impacts the interface the mass transfer coefficient reaches a maximum and then decays in time as the near interface fluid saturates by diffusion of the solute – till the region is eventually refreshed by another sweep.

In the bottom of the figure the Reynolds stress and the vertical fluctuating velocity are shown as time proceeds and in a Lagrangian frame moving with the interface velocity. When they are both negative, a sweep is impacting the interface. In the center Figure, the corresponding mass transfer velocity is shown and compared to the values predicted by surface renewal theory. The top figure shows the total mass flux over time. The dotted curve in the center and top figures are computed using, respectively $\sqrt{D/(\pi t)}$ and $2\sqrt{(Dt)/\pi}$. They represent the instantaneous flux and the total flux *i.e.* the time integral of the instantaneous flux, for transient diffusion into a stagnant media.

It appears that the mass transfer velocity increases when a sweep is present at the interface. The mass transfer velocity decays with the expected -1/2 exponent. Also the total mass transfer, *i.e.* the integral of β^+ over the time period increases as $t^{1/2}$.

Supported also by the results of the quadrant analysis, a model based on surface renewal theory seems appropriate for liquid side mass transfer. Sweeps appear to coincide with the renewals that control the mass transfer process, and the time history of β^+ in Figure

7 also supports this hypothesis.

On the gas side, at first glance, it seems that this assumption would be less well founded. In fact we observed that all large vertical (interface-normal) velocity fluctuations are responsible for high mass transfer rates. Large vertical fluctuations are, however, mainly related to the bursting process thus also supporting parametrizations based on surface renewal-type models with both sweeps and ejections being important.

Consider first the liquid side. In this case we use a parametrization proposed by Banerjee (1990). Consider the simple surface renewal expression, $\overline{\beta} = (D/\tau)^{1/2}$, and assume that $\tau^+ = 30$ to 90 $(\nu/u_\star^2)$, where τ, as discussed before is the time ranging between sweeps and bursts. We then obtain the relation,

$$\frac{\overline{\beta_l} Sc^{0.5}}{u_l^\star} = 0.108 \text{ to } 0.158 \qquad (2)$$

This expression is compared with simulation results over a large range of Sc number [Figure 3.a] and good agreement is found for the high Sc number cases. From our DNS we obtain a value of $T^+ = 50$. This gives a coefficient of 0.14, that is also reported in Figure 3.a.

Equation 2 has also been compared with wind-wave tank data for SF_6 transfer rates from Wanninkhof and Blivens (1991) in De Angelis (1998), and good agreement is found.

Turning now to the gas side, the gas sees the liquid much like a solid surface as discussed earlier. So a form of the surface renewal theory modified for such applications, *e.g.* by Banerjee (1971) amongst others, is necessary. This leads to a different dependence in the Schmidt number, and the modified expression is:

$$\frac{\overline{\beta_g} Sc^{2/3}}{u_g^\star} = 0.07 \text{ to } 0.09 \qquad (3)$$

Figure 3.b compares the expression with DNS results. It is clear that the Schmidt number dependency is correctly predicted, and the numerical values are within the range of Equation 3. The lower bound of Equation 3 compares well with the moisture transfer data of Ocampo-Torres *et al.* (1994) as reported in De Angelis (1998).

On the gas and liquid sides the value of β^+ changes slightly with wave amplitude. Reynolds stresses and mass transfer velocity increase on the liquid side and decrease on the gas side only slightly. Therefore the correlations still capture the main transfer mechanisms when capillary waves form.

CONCLUSION

By using Direct Numerical Simulation, it is possible to correctly compute values of the mass transfer velocity for a relevant range of Sc number. Once the results of DNS are available, it is possible to test hypotheses and mechanisms governing mass fluxes. We could clarify, both by visual inspection of the velocity field, and by the use of statistical tools, like quadrant analysis, the main features of turbulent structure on the gas and liquid side. Then we could correlate mass flux with the turbulence structure and detect the renewal events that drive the mass transfer processes. As result of this study, we can propose parametrizations that predict the mass transfer, without any adjustable parameters. For this problem, DNS has proved to be a powerful modeling tool.

REFERENCES

S. Banerjee, 1971, "A note on Turbulent Mass Transfer at High Schmidt Numbers", *Chem. Eng. Science*, 26, pp. 989-990.

S. Banerjee, 1990, "Turbulence structure and transport mechanisms at interfaces", *Proceedings of the Ninth International Heat Transfer Conference*, Jerusalem, Israel, pp. 395-417.

V. De Angelis, 1998, "Numerical Investigation and Modeling of Mass Transfer Processes at Sheared Gas-Liquid Interfaces", PhD Dissertation, University of California at Santa Barbara.

S. Komori, R. Nagaosa and Y. Murakami, 1993, "Turbulence Structure and Mass Transfer Across a Sheared Air-Water Interface In Wind-Driven Turbulence", *J. of Fluid Mech.*, 249, pp. 161-183.

Garrar, J.R., 1977, "Review of drag coefficients over Oceans and Continents", *Mon. Weather Rev.*, 105, pp. 915-929.

P. Lombardi, V. De Angelis and S. Banerjee, 1996, "Direct numerical simulation of near-interface turbulence in coupled gas-liquid flow", *Phys. Fluid*, 8, pp. 1643-1665.

M.J. McCready and T. Hanratty, 1985, "Effect of air shear on gas absorption by a liquid film", *AIChE Journal*, 31(12), pp. 2066-74.

M. Rashidi and S. Banerjee, 1990, "The effect of boundary Conditions and Shear rates on Streaks formation and breakdown in Turbulent channel flow", Phys. Fluid, A2, pp. 1827-38.

F.J. Ocampo-Torres, F.J. Donelan, J.M. Woollen and J.R. Koh, 1994, "Laboratory measurements of Mass Transfer of Carbon Dioxide and water Vapor for Smooth and Rough flow conditions", Tellus Series B, 46, p. 16-28.

R.H. Wanninkhof and L.F. Bliven, 1991, "Relationship between gas exchange, wind speed, and radar backscatter in a large wind wave tank", J. of Geophys. Res., 96(C2), pp. 2785-2796.